J Sol-Gel Sci Technol (2017) 81:791–796
DOI 10.1007/s10971-016-4244-4

ORIGINAL PAPER: SOL-GEL AND HYBRID MATERIALS FOR BIOLOGICAL AND HEALTH (MEDICAL) APPLICATIONS

Biocompatible superhydrophobic coating material for biomedical applications

Satish A. Mahadik[1,2,3] · F. Pedraza[1] · Sarika S. Mahadik[3] · Brahmanand P. Relekar[3] · Sagar S. Thorat[4]

Received: 31 March 2016 / Accepted: 18 September 2016 / Published online: 25 October 2016

Abstract Biomaterials and wettability have played a crucial role in the biocompatibility with a host matrix of body fluid and cells. We discuss designing superhydrophobic biomaterials for novel applications such as temporally implant, contact lenses, controlled drug release coatings, coating on medical instruments, etc. Such Superhydrophobic coating surfaces were created with the simple dip coating method by single step base catalyst sol-gel method. Methyltriethoxysilane/trimethoxymethylsilane-based deposition at different dip periods introduces interesting properties in the region, including superhydrophobicity, biocompatibility and transparency. This works reveal the impact of interaction bone marrow mesenchymal stem cells and surface free energy on the biocompatibility of superhydrophobic biomaterial.

Graphical Abstract

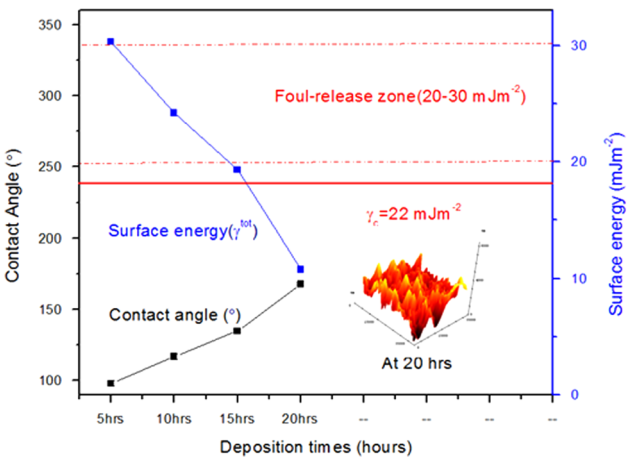

Keywords Superhydrophobicity · Material-cell interaction · Sol-gel · Biocompatibility · Dip coating method

✉ Satish A. Mahadik
superhydrophobicmaterial2100@gmail.com

[1] Laboratoire des Sciences de L'Ingénieur pour l'Environnement (LaSIE, FRE-CNRS3474), Université de La Rochelle, Avenue Michel Crépeau, La Rochelle cedex 01 17042, France

[2] Department of Physics, Adarsha Institute of Technology and Research Center, Vita 415311, India

[3] Department of Physics, Shivaji University, Kolhapur 416 004, India

[4] Organic Chemistry Division (OCD), CSIR-National Chemical Laboratory, Dr. Homi Bhabha Road, Pune 411008, India

1 Introduction

Superhydrophobic surfaces (contact angle ≥ 150°, and sliding angle ≤ 10°) designed so that drops do not stick to them, but instead jump off have raised significant attention because of their ability to self-clean, anticorrosion, drag reduction, stay non wettable, resist icing, improving blood compatibility and antifouling surfaces [1]. Nowadays, there has been much research interest in producing biomaterial with controlled wettability, which have surface free energy beyond the foul releasing zone (20–30 mJm^{-2}), because of

their importance in biocompatibility research as well as practical applications of biometrics such as dental implants, sutures, and many medical devices [2]. Superhydrophobic surfaces have successfully designed for non sticky cookware, water repulsive coatings, antifouling surfaces, microfluidic devices, transparent, antireflective, and self cleaning smart glasses, anticorrosive surfaces [3–6]. Earlier research work shown that superhydrophobic surfaces could be most useful in numerous biomedical-related areas such as anti-bioadhesion applications to avoid protein adsorption and cell adhesion on a surface [7–9].

Several artificial materials are being employed as implants in all fields of medical science. The physicochemical properties of the implant surface like surface topography, surface free energy (SFE) are of ground importance for the specific adhesion, spreading and growth of cells [10]. Synthetically designed materials such as polymethylmethacrylate, cellulose acetate, Dacron, polyester-urethanes, polyethylene glycol have also been used as most prominent biomaterials. Generally, large number of efforts have been focused on organic based superhydrophobic surfaces, but typically chlorine and fluorine-based material do not exhibit biocompatibility due to cytotoxicity [11, 12]. Realization of such artificial biocompatible surfaces with superhydrophobicity is a challenging issue as recent studies demonstrated. For instance, Gu et al. fabricated inverse opal films with superhydrophobic nature (CA = 155°) [13]. However, the fabrication process of the opal structure is long and requires precise high temperature conditions (450 °C). In 2006, Jiang et.al described polystyrene based biocompatible coatings, but they show a poor repellency nature [14]. Sun et al. proved that the biocompatibility could be mostly enhanced by introducing particular nanostructure to make the poly (carbonate urethane) based superhydrophobic coatings [15]. Khorasani and Mirzadeh indicated the modified polydimethylsiloxane (PDMS) surface endowed with superhydrophilic or superhydrophobic nature exhibited better biocompatibility compared with pure PDMS [16]. Unfortunately, this type of surfaces shows poor wettability properties, requites costly materials and relatively complex synthesis process. In addition, only few reports are found on the growth or interaction of cells with artificial ultrahydrophobic surfaces [17–21]. The method of coating by sol-gel dip is advantageous as it offers simple synthesis process at room temperature without the use of any complicated instruments [22]. It is also claimed as eco-friendly, easy to scale up with tailored surface chemistries for arranging expected properties and applicability as a biomaterial.

In this work, we demonstrate the sol–gel dip coating method as a simple approach to enhance hydrophobicity by introducing nanostructured surface chemistry composed of silica networks on a glass substrate. In this scheme, the surface free energy of silica coating surface has been successfully reduced by increasing dipping periods. Furthermore, the effects of the dipping periods on topography, SFE with polar components, work of adhesion and biocompatibility of the coating material have been investigated.

2 Experimental section

2.1 Materials

Ordinary glass substrates with sizes of 75 mm × 25 mm × 1.45 mm were obtained from the blue star Mumbai. All chemicals, reagents and solvents were used further synthesis without any purification process. Methyltriethoxysilane (MTES (99 %, Sigma-Aldrich Chemie, Germany), and trimethoxymethylsilane (TMMS) (99 %, Sigma-Aldrich Chemie, Germany) were used as silica precursor. Ammonia (NH_3, Sp.Gr.0.91 Qualigens Fine Chemicals, Mumbai) was used as base catalyst and methanol (S. D. Fine-Chem Ltd., Mumbai) as solvent for sol–gel reaction. The bone marrow cell named as mesenchymal stem cells (MMSCs) were obtained from the local meat market for the conducting adhesion experiments in the laboratory. The streptomycin sulfate salt (100 µg/ml, Sigma Aldrich Chemie, Germany) and Penicillin G potassium salt (100 U/L, Sigma Aldrich Chemie, Germany) were used as bioreagent for cell culture.

2.2 Synthesis and characterization of coatings

The superhydrophobic coating was synthesized by dipping deposition via sol–gel route at room temperature. The hydrophobic coating alcosol was prepared at an optimized molar ratio of MTES: TMMS:CH_3OH: H_2O at 1:0.15:12.71:3.58, respectively, with 13 M NH_4OH as a base catalyst at room temperature (27 °C). A single step-base catalyzed sol-gel process was followed to prepare the coating sol solution. The detail synthesis procedure for superhydrophobic dip coating was described in our previous work [10].

A Fourier-transformed infrared spectrometer (Perkin-Elmer, Model no. 783, USA) and Fourier-transformed Raman spectrometer (Bruker, Multi RAM Stand-Alone FT-Raman, Germany) were used for the study of the chemical structure of the dip coated silica materials. The surface topography of the dip coated surfaces was observed using a Nanoscope E (Digital Instruments, USA) atomic force microscopy. The coating samples were annealed in furnaces at 100 °C temperature (Neytech. VULCAN Benchtop Model 3-550 USA). Contact angle measurements were carried out by the sessile drop method using advanced

contact angle meter (Rame hart, model 501F1, USA) apparatus and double distilled water droplets (5 µL). A sliding angle measurement performed by tilting plate method with drop volume about 5 µL. To measure the contact angle hysteresis (CAH), we also precise the receding contact angle (RCA) of water by sucking the liquid from the left drop at a size rate of 0.2 μls^{-1}. An experimental data were represented as mean ± standard deviation (SD) for $n = 5$. Optical transmission was measured over the range of 350–1000 nm using a UV-Vis spectrophotometer (Shimadzu, model: UV-1800, Japan).

3 Result and discussions

3.1 Surface topography

Fig. 1 displays the 3D surface morphologies of MTES/TMMS based coatings, which were deposited at different dip periods ranging from 5 to 20 h. Facet spikes were shown in the coating deposited for 5 h, however, the coating deposited at 10, 15, and 20 h consisted of sharp spikes. The increase of dipping time simultaneously enhances the roughness of surface and the hydrophobicity properties of the coating surface.

As hypothesized, all the coatings are rough: surface roughness progressively ranges between 217 ± 4 and 717 ± 8 nm with an increasing dipping period. Also, the contact angle and roughness for all coatings happened to be significant, as shown in Table 1. The hierarchical morphology enables the surface to repel liquid. As a result, the surface roughness could be increased with the increase of dipping periods. From topography of analysis, it is clear that increased dipping periods responsible for development of hierarchical morphology, which is beneficial for anti-wetting protein surface [23].

3.2 Surface energy measurements superhydrophobic of surfaces

We also analyzed the wetting behavior of a coating surface by finding out contact angles of three liquids probe (water, ethylene glycol, diiodomethane) and quantifying the surface free energy, polar components, and work of adhesion at the solid liquid interface using the van Oss–Good–Chaudhury method [24]. As assumed, all dip coated surfaces showed progressively higher water contact angles range from 98°, 115°, 135°, 142°, and 168° with increasing dipping periods from 5,10,15, and 20 h as shown in Table 1. Also, the surface free energy and work of adhesion of the silica coating for different dipping time was found to be significant, as shown in Fig. 2. Also, there is minor variation in the polar component of the surface free energy (or improved hydrophobicity) over the entire dipping period, which is consistent with the formerly reported works, but the mechanism behind its improved wettability behavior has not been deply discovered in term of polarity nature of surface [25, 26]. We also systematically measured CAH on a surface of coatings and found it to range between 39 ± 2° and 4 ± 1°. We attribute this drastically low value of CAH to the homogeneous nature arising from higher RMS surface roughness that cannot allow the droplet to pin on the hierarchical textures. From above observation it is clear that, as the works of adhesion of the coatings were dropped progressively with dipping periods because of evolution of hierarchical texture with hydrophobic nature.

3.3 FT-Raman analysis

The chemical analysis of coating material was supported by FT-Raman spectra as shown in Fig. 3, as a functional group evolution at 20 h dipping period. The Broad peaks at 473 and 801 cm^{-1} arose from the asymmetric stretching vibrations of Si–O–Si bonds [27, 28]. This vibration is assigned to the Si–O–Si symmetrical stretching of the cluster, a cluster-breathing mode. It is shown here; there is a condensation of asymmetric stretching modes of the $Si–CH_3$ at 744 and 1413 cm^{-1}. The more intense vibration peaks assigned to the C–H from $–CH_3$ bounds of the ORMOSIL network. There are the symmetric and asymmetric stretching vibration modes of the C–H bonds corresponding to 2913 and 2974 cm^{-1}, respectively [29–31]. It thus appears that condensation of $Si–CH_3$ can be responsible for the superhydrophobicity.

3.4 Optical transmittance

Optical transmittances of coatings with hierarchical textured surfaces changed with thickness and roughness. The roughness of the coatings increased from 217 ± 4 nm to 717 ± 8 nm by varying the dipping time while achieving superhydrophobicity order and transparency (Fig. 4). Up-scaling the structure sizes have a strong effect on the visible light intensity. Fig. 4 compares UV-Vis-NIR transmission of a coating deposited on both major surfaces at various dipping periods at normal incidence (colored lines), and to uncoated glass substrates (black line). The rough textures (717 ± 8 nm) at 20 h show a low transmittance arising from Mie scatterings effect due to hierarchical surface morphology and absorptive coupled resonances of the ordered thickness with increasing dipping time [11], optical light transparency is significantly influenced by their roughness and thickness variation are clearly depicted in Table 1.

The increase in thickness results in rougher surfaces that lead to a drastic fall in optical transmittance. However, thick hierarchical textures develop optical opacity because of

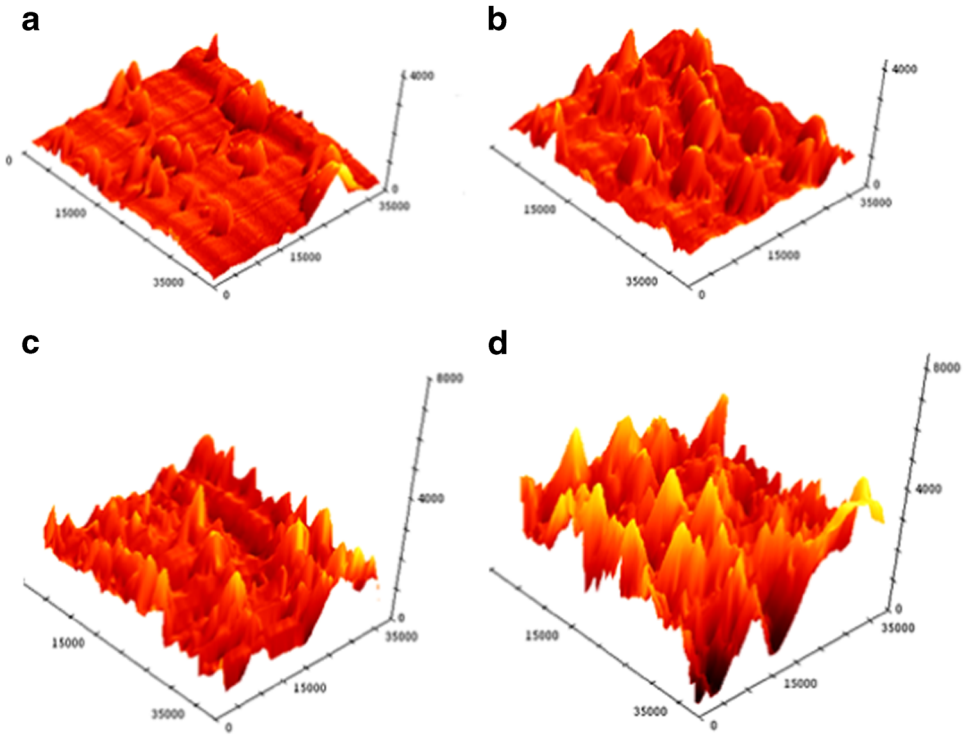

Fig. 1 Surface topography evolution at different deposition times **a** 5 h, **b** 10 h, **c** 10 h, and **d** 20 h

Table 1 Measured transparency, thickness, roughness, contact angles with three liquids and CAH on silica coatings deposited at different dipping periods

Dipping hours	Visibility at 537 nm	Thickness (nm)	Roughness (nm)	Advancing contact angle			CAH $\theta_{Adv}-\theta_{Res}(^\circ)$
				Water	Ethylene glycol	Diiodomethane	
5	98.68	258 ± 10	217 ± 4	98 ± 4°	63 ± 3°	13 ± 1°	39 ± 2°
10	90.88	414 ± 26	331 ± 6	115 ± 3°	71 ± 4°	28 ± 1°	27 ± 2°
15	81.70	637 ± 18	411 ± 4	135 ± 3°	77.5 ± 4°	36 ± 2°	16 ± 1°
20	68.38	980 ± 21	717 ± 8	168 ± 1°	96 ± 6°	60 ± 4°	4 ± 1°

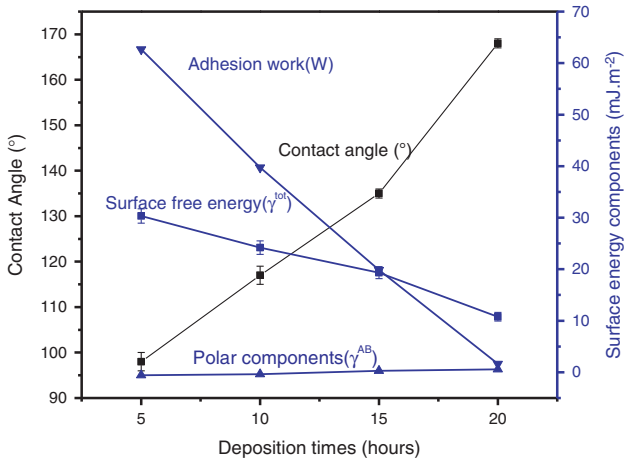

Fig. 2 Surface wetting properties of silica coatings at different deposition period; Advancing water contact angle (*left y axis*) and the surface free energy, work of adhesion, and polar component of the surface free energy (*right y axis*) of coating surface

their structural features, which absorb light energy. From a coating surface roughness of 217 ± 4 and 331 ± 6 nm, no loss of transmitted light is noticed and the coatings surfaces appear as antireflective and transparent as regular glass after 5 and 10 h of immersion, respectively. For surface roughness of 411 ± 4, 541 ± 5, and 717±8 nm, the coating lost optical transmission of up to 25 %. Transmission can be reduced because of the large gradient of the refractive index in the hierarchical textures. Because of reducing the transmission from the silica coating surface, the thickness and roughness of the hierarchical silica coatings were increased. We assign the balanced transmission to the enhanced hydrophobicity contrast of the coated sample compared with the bare glass substrate.

3.5 In vitro biocompatibility test

To evaluate the in vitro biocompatibility of coating material (MTMS /TMMS) carried out the method according to

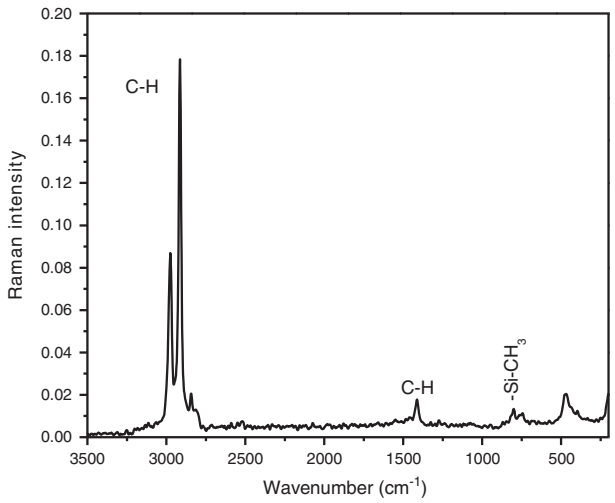

Fig. 3 Surface chemical composition by Raman analysis for superhydrophobic coating at 20 h

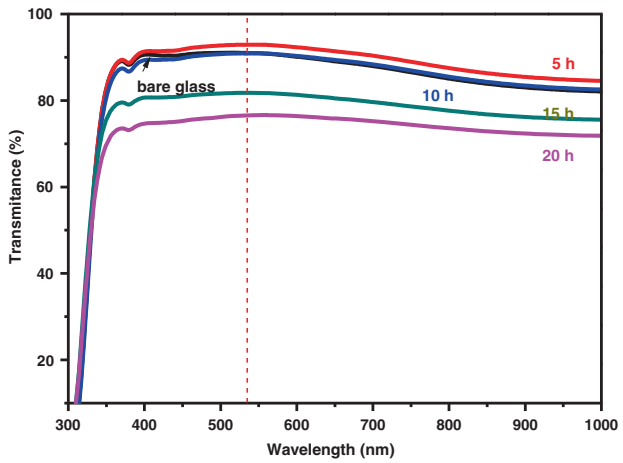

Fig. 4 Optical transmittance for silica coatings at different dipping times

earlier reports [32]. The optical inspection is performed using Atomic force microscopy and optical microscopy provides useful information about cell morphology, growth of cells and adhesion quality of bone marrow mesenchymal stem cell (BMMSC) on superhydrophobic material. The 3D surface topography and optical results reported in Fig. 5 (a–b) clearly show that superhydrophobic coating material as a base for BMMSC cell culture examined after incubation for 7 days. It can be seen that BMMSC cells are adhered to the material and flattened growth morphology with minor filopodia. In addition, it is obvious from the Fig. 5(a–b) show the cells homogeneously grow on the material and partially contact with the superhydrophobic coating material. It is established the (MMSCs) cell adhesion and activation play a crucial role in biocompatibility through superhydrophobicity and surface roughness of coating material. Such low surface free energy (10.78 mJm^{-2}) and minimum work adhesion (1.69 mJm^{-2}) material is often used for temporary medical implants, as the low adhesion makes them easier to remove later like coating on contact lens, metal rod and various medical instruments etc. [33, 34]. It is consistent with the earlier reported critical surface free energy limit ($\gamma_c = 22\ mJm^{-2}$) for spreading liquid substrate for water interface. All above observations in this work suggest the superhydrophobic materials holds a minimum adhesion to BMMSC and a capability to inhibit the introduction and growth of the attached platelets, which is whispered to be capable to effectively prevent thrombosis. From the results discussed above, it could be concluded that such superhydrophobic coating material is safe and effective materials for BMMSC cell contact applications can now be consistently preferred based on in vitro biocompatible test.

4 Conclusions

This work has successfully substantiated that biomaterial surfaces exhibiting superhydrophobicity crucial role in

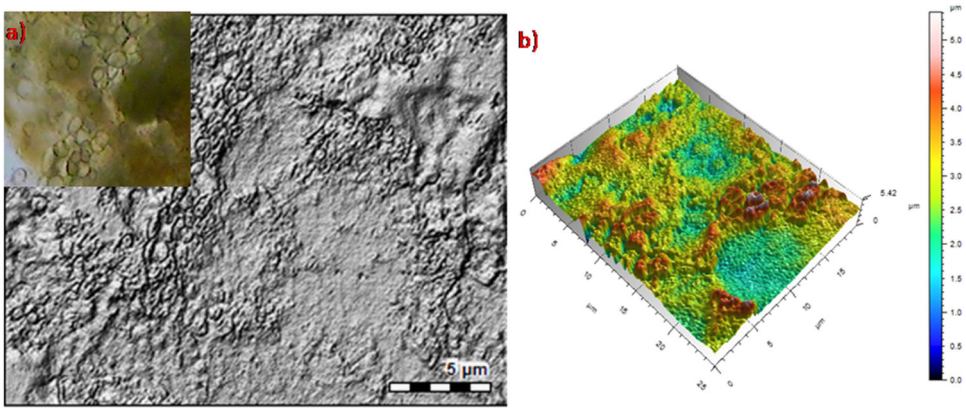

Fig. 5 The topographical sudy of the MMSCs adheres and spreading on superhydrophobic material after 7 days **a** 3D surface visulasisation cell growth (inset optical image). **b** psudo color view of topography

biocompatibility. The temporary metal implant, contact lenses and medical instrument surfaces need an appropriate surface low energy and superhydrophobic surface entities, because excessively lower hydrophobic surfaces enhance cell affinity and becomes very difficult to remove. Although observation from in vitro evaluations of superhydrophobic biomaterials may aid in predicting some of their behavior in vivo, it would be helpful in many applications, where a need for biocompatible with minimum cell interaction is highly desirable.

Acknowledgments The author acknowledges the department of physics, Shivaji University Kolhapur, India for providing the experimental facility under the DST phases-3.

Compliance with ethical standards

Conflict of interest The authors declare that they have no competing interests.

References

1. Lee Y, Park S, Kim K, Lee J (2007) Adv Mater 19:2330–2335
2. Langer R, Tirrell DA (2004) Nature 428:487–491
3. Jeri AH, Jonas DM, Michael FR (2002) Nater Mater 1:59–63
4. Whitesides GM (2006) Nature 442:368–373
5. Blossey R (2003) Nat Mater 2:301–306
6. Li K, Ju J, Gao S, Jiang L (2013) Nat Commun 4:2276–2283
7. Chen Z, Hao L, Chen C (2012) Colloids Surf A 1:1–7
8. Langer R, Tirrell DA (2004) Nature 428:487–492
9. Hou X, Wang X, Zhu Q, Bao J, Mao C, Jiang L, Shen J (2010) Colloids Surf B 80:247–250
10. Xu LC, Siedlecki CA (2007) Biomaterials 28:3273–3283
11. Mahadik SA, Rao AV (2010) Appl Surf Sci 257:333–339
12. Nimittrakoolchai O, Supothina S (2008) Macromol Symp 264:73–79
13. Gu ZZ, Uetsuka H, Takahashi K, Nakajima R, Onishi H, Fujishima A, Sato O (2003) Angew Chem Int Ed 42:894–897
14. Ge H, Song Y, Jiang L, Zhu D (2006) Thin Solid Films 515:1539–1543
15. Sun TL, Tan H, Han D, Fu Q, Jiang L (2005) Small 10:959–963
16. Khorasani MT, Mirzadeh H (2004) J Appl Polym Sci 91:2042–2047
17. Oliveira SM, Song W, Alves NM, Mano JF (2011) Soft Matter 7:8932–8941
18. Shi J, Alves NM, Mano JF (2008) Bioinspir Biomim 3:034003–034010
19. Song W, Veiga DD, Mano JF (2009) Adv Mater 21:1830–1834
20. Alves NM, Shi J, Oramas E, Santos JL, Toma SH, Mano JF (2009) J Biomed Mater Res Part A 91A:480–488
21. Ishizaki T, Saito N, Takai O (2010) Langmuir 26:8147–8154
22. Mahadik SA, Vhatkar RS, Wagh PB (2013) Appl Surf Sci 277:67–72
23. Lourenço BN, Marchioli G, Song W, Mano JF (2012) Biointerphases 7:1–4
24. Good RJ (1992) J Adhes Sci Technol 6:1269–1302
25. Kubiak KJ, Wilson MCT, Mathia TG (2011) Ph Carval Wear 271:523–528
26. Schmidt P, Bellot-Gurlet L, Slodczyk A, Fröhlich F (2012) Phys Chem Miner 39(6):455–464
27. Mahadik SA, Pedraza F, vhatkar RS (2016) J Alloys Compd 663:487–493
28. Mahadik SA, Rao AV (2012) J Sol-Gel Sci Technol 62:490–494
29. Mahadik SA, Pedraza F, Hegade ND, Wagh PB (2013) J Colloid Interface Sci 405:262–268
30. Mahadik SA, Rao AV (2012) J Sol-Gel Sci Technol 63:580–586
31. Mahadik SA, Pedraza F (2016) J Sol-Gel Sci Technol 78:475–481
32. Jagadale PN, Bamane SR (2013) Mater Sci-Poland 31:269–275
33. Krasteva NA, Toromanov G, Hristova KT (2010) J Phys Conf Ser 253:012079–012085
34. Garretta TR, Bhakoob M, Zhanga Z, (2008) Prog. Nat Sci 18:1049–1056